CrystEngComm

Precipitation Dominated Thin Films of Acetaminophen Fabricated by Meniscus Guided Coating

Journal:	*CrystEngComm*
Manuscript ID	CE-ART-10-2021-001437.R1
Article Type:	Paper
Date Submitted by the Author:	15-Nov-2021
Complete List of Authors:	Guthrie, Stephanie; University of Virginia, Chemical Engineering Smith, Natalie; University of Virginia, Chemical Engineering Conley, Ashley; University of Virginia, Chemical Engineering Smilgies, Detlef; Cornell University, CHESS Giri, Gaurav; University of Virginia, Chemical Engineering

Precipitation Dominated Thin Films of Acetaminophen Fabricated by Meniscus Guided Coating

Stephanie Guthrie[1], Natalie Smith[1], Ashley Conley[1], Detlef-M. Smilgies[2], Gaurav Giri[1]

[1]Department of Chemical Engineering, University of Virginia, Charlottesville, Virginia, 22904, United States
[2]Cornell High Energy Synchrotron Source (CHESS), Wilson Laboratory, Cornell University, Ithaca, New York 14853, United States

Corresponding author: Gaurav Giri, gg3qd@virginia.edu

ABSTRACT

Recently, meniscus-guided coating (MGC) has been utilized for small molecule pharmaceutical crystallization and has demonstrated the ability to direct the formation of crystal polymorphs. However, the traditional coating regimes (evaporative and Landau-Levich) do not provide adequate control over the crystal size or shape - specifically the formation of small and low-aspect ratio crystallites is desirable for pharmaceutical applications. In this work, MGC processing conditions are adjusted to achieve three distinct film morphologies of acetaminophen from aqueous solutions. The morphologies are characterized using polarized optical microscopy and scanning electron microscopy. Notably, we identified a set of processing conditions that results in uniform microcrystal formation due to rapid evaporation and precipitation. Deposits created with this technique produce crystallites with an average diameter of 6.9 ± 2.4 μm with nearly monodisperse size distributions. X-ray diffraction was used to assess polymorphism and crystal texture in the thin films as a function of processing conditions, revealing that the microcrystals are heterogeneously nucleated and preferentially oriented on the substrate. This work contributes new insight to processing techniques which may be relevant to continuous pharmaceutical manufacturing efforts by obtaining preferred morphologies.

INTRODUCTION

The pharmaceutical industry has made advances towards implementing continuous processes for drug production.[1,2] Guided by quality by design, continuous manufacturing operations provide an opportunity to improve process efficiency and product quality.[3] One challenging step in continuous pharmaceutical manufacturing is associated with continuous crystallization of pharmaceutical compounds.[4] Continuous crystallization technologies are desired

due to ease of integration with upstream and downstream unit operations, as well as more uniform crystallization conditions compared to batch crystallization.[5] In addition, traditional batch crystallization approaches are prone to batch-to-batch variability with regards to product recovery and quality.[6] There is a persistent need to develop scalable crystallization technologies which can provide control over critical characteristics of the final crystal product.[7]

Controlling crystal polymorph, size, shape and morphology while using continuous and scalable manufacturing techniques has become an active field of research.[8–12] The ability to control crystal size, shape and crystal size distribution (CSD) is a necessity due to the direct relationship between the morphology of the pharmaceutical compound to the resultant biological performance.[13] For example, smaller crystals have been shown to have faster dissolution rates compared to larger crystals due to increased surface area relative to volume.[14]

Crystal shape impacts dissolution profiles as well.[15] Further, low aspect ratio crystals or aggregate shapes, such as spheres, have superior flowability for ease of processing.[15] These low aspect ratio shapes are therefore desirable from a processing standpoint compared to needles or platelets. Multiple technologies have been studied to create optimal crystal morphologies. For example, supercritical CO_2 facilitated spray drying has been successfully applied to the continuous production of spherical crystals.[16] Spray drying has been used to create micro- and nano-crystals, for ease of dissolution.[17] The incorporation of additives in crystallization processes can also change crystal morphology during crystallization and produce low aspect ratio crystal shapes.[18] Spincoating and dropcasting are thin film solution processing techniques that have produced unique crystal morphologies and polymorphs, however these techniques are not easily scalable for use in continuous processes.[19–21]

Another technique that has been utilized to manufacture organic molecule thin film crystals is based on meniscus-guided coating (MGC).[22] One MGC technique, termed solution shearing, is useful for controlled deposition of thin films from liquid phase solutions.[23] The coating parameters (coating speed and substrate temperature) are used to create solid thin films with controllable

thickness and coverage by modulating deposition and evaporation timescales.[23] Previously, solution shearing has been utilized to control polymorphism and crystal morphology in organic semiconductor small molecules.[24,25] The technique has also gained popularity for fabrication of perovskite thin films.[26] Recently, solution shearing was applied to pharmaceutical molecules including acetaminophen, glycine, ellipticine and aspirin[27,28] and was found to provide control over polymorphic phases. At this time, there are few examples of MGC being applied for pharmaceutical crystallization relative to the number of studies in polymers and organic semiconductors. By identifying solution shearing parameters to control the crystallization of pharmaceutical molecules, evaporative crystallization itself can be integrated into the continuous manufacturing of pharmaceutical compounds, thus streamlining drug product production.[29]

In addition, understanding MGC parameters that provide desired morphologies and polymorphs simplifies downstream production requirements. For pharmaceutical crystallization, the production of microcrystals with low aspect ratios is desired for enhanced biological performance. In addition, free flowing microcrystals allow for less clogging during crystallization processes. Also, thin film formulations are an alternative to oral tablet formulations, when a tablet or liquid formulation is not possible.[30] Oral thin films provide rapid drug delivery through dissolution of the active pharmaceutical ingredient in the mouth, an advantage for patients who have difficulty swallowing tablets and capsules.[30] Thus, there has been a surge in development of thin film prototypes of different APIs, such as diclofenac sodium, ellipticine, caffeine and hydrocortisone among others.[28,31,32] MGC could be useful for the fabrication of thin film formulations with high throughput and scalability.

In this work, we studied the applicability of solution shearing as a scalable processing technique for the continuous crystallization production of low aspect ratio microcrystals in a thin film. Meniscus guided coating techniques have previously been shown to be useful to make thin film pharmaceutical formulations, such as multilayer thin films.[28] Although previous work has shown that numerous crystal morphologies can be isolated using solution shearing, there has

been no study demonstrating control over the formation of low aspect ratio microcrystals.[27,28] Here, we utilize an acetaminophen and water system and processing temperatures above the boiling point of the solvent for the first time in solution shearing, to create uniform microcrystals with low aspect ratios. We show that solution shearing at temperatures above the boiling point of the solvent allows us to access a thin film morphology that has not been obtained previously using MGC. We demonstrate that elevated temperature and slow coating speed produce a distinct morphology for films created using MGC techniques, termed herein as a precipitation regime for crystallization. Utilizing solution shearing with these unconventional operating parameters produced a nucleation dominated crystallization regime with a continuous production of microcrystals that are 6.9 ± 2.4 μm in diameter. Within each sample, the crystal populations are nearly monodisperse (average sample polydispersity index = 0.12). Grazing incidence wide angle X-ray diffraction (GIXD) was used to assess the crystal texture within thin films. We found that crystallites within the microcrystalline films are preferentially oriented on the substrate. This finding constitutes a significant advancement to the field of pharmaceutical crystallization and other fields where organic molecule crystallization is important, such as in the fields of organic electronics and energetic materials.

MATERIALS AND METHODS

Solution Preparation: Acetaminophen (98%, Sigma-Aldrich) solutions were prepared with ultrapure water at room temperature (23 °C) with concentrations of 1, 5, 10, 14 mg mL^{-1}. Solutions were filtered through a 0.2 μm filter prior to use.

Solution shearing device: Films were created using an in-house solution shearing machine. The equipment contains a custom designed and machined aluminum base with heating cartridges (McMaster-Carr) for thermal control. J-type thermocouples (McMaster-Carr) and heating components are interfaced with a PID controller (Omega Engineering Inc.) to ensure temperature is maintained at the set point. The aluminum block contains a vacuum connection to secure the substrate to the heated aluminum stage, ensuring good thermal contact. The shearing

blade is secured via vacuum to a blade holder (custom) and is connected to angle/yaw (Opto Sigma Corporation) and height (Edmund Optics) micromanipulators and a motorized linear driver (Zaber Technologies) to control the speed of translation across the substrate.

Shearing Blade Functionalization: A functionalized silicon wafer edge was used as a shearing blade. The shearing blade was functionalized with trichloro(octadecyl)silane (OTS) by activating the cleaned wafer in a UV/ozone cleaner and placing the activated wafer in a 3% OTS/ethanol solution in a crystallization dish for 30 minutes. The functionalized wafer was cured on a hot plate set to 90 °C for 1 hour, and then sonicated for 10 minutes to remove any physically adsorbed material on the wafer surface. The contact angle (**SI Figure 1**) was found to be approximately 87°, confirming that the blade had improved hydrophobic character relative to untreated silicon (contact angle approximately 30°).

Thin film fabrication: Silicon substrates were cut into 1 cm^2 pieces and were cleaned with toluene, acetone, water and IPA, and then dried under pressurized air. Clean wafers were placed in a UV/ozone cleaner (Bioforce ProCleaner Plus) for 10-15 minutes prior to their use. This treatment facilitates surface wetting of the aqueous solution. To create thin films, the desired temperature was set and applied to the substrates, ranging from 70 - 120 °C and shearing speeds were set to 0.01 - 3 mm s^{-1} in this work. For microcrystal morphology, speeds of 0.01 - 0.05 mm s^{-1} were explored.

Scanning Electron Microscopy: Samples were sputter coated with a gold palladium layer using a Technics Hummer sputter coater prior to imaging. A FEI Quanta 650 scanning electron microscope (Thermo Scientific) was used with a 10 mm working distance and an accelerating voltage of 5 kV.

Polarized optical microscopy: A Zeiss Axio Imager A.1 optical microscope (Carl Zeiss AG) with two polarizers oriented orthogonally produced linearly polarized light for characterizing thin film alignment and isotropy. Films were imaged using a Zeiss Axiocam 503 Color camera (Carl Zeiss AG).

Image Analysis: Crystal sizes were measured in ImageJ by drawing a line across the largest dimension of a crystal grain and using the measure feature. At least 40 crystals were measured for each sample, and at least three samples were created at each condition. Crystal size distributions were plotted on histograms. For each sample, the polydispersity index (PDI) was determined as $PDI = \left(\frac{Standard\ Deviation}{Average}\right)^2$.[33,34]

Interferometry: A Zygo NewView 730 white light interferometer (Zygo Corporation) was used to determine the thickness of the films.

Grazing Incidence Wide Angle X-Ray Diffraction: Grazing incidence wide angle X-ray diffraction was used to characterize thin film polymorphism and texture. Diffraction patterns were gathered at the Cornell High Energy Synchrotron Source (CHESS) at the former D-1 beamline. Incidence angles were set to 0.15°. The beam energy was 10.67 KeV and sample to detector distance was 175 and 177 mm. A Pilatus 200K detector was positioned to image one quadrant (Cartesian quadrant 2) of the diffraction pattern, with the beam center in the bottom right corner. The crystallographic orientation of crystals in the thin film was determined using peak indexing, with the indexGIXS software package developed by Smilgies et al.[35]

The crystal structure of acetaminophen form I was simulated with the program Mercury by the Cambridge Crystallographic Data Centre (CCDC) using previous reports from Nelyubina et al (CCDC deposition 754966, HXACAN30).[36] Form II was simulated from Nichols et al. (CCDC deposition 135452, HXACAN08).[37]

The texture in the film was characterized quantitatively by examining the distribution of diffraction intensity for the (110) crystal plane on a 2D diffraction image. The degree of crystal orientation was quantified by determining the amount of scattering that occurred in the expected (oriented) region of reciprocal space relative to the total amount of diffraction associated with the (110) plane. This approach was previously utilized by Chen et al. to characterize the degree of preferential orientation in perovskite films.[38]

For acetaminophen form I, the (110) plane is located at $q = 0.86\,\text{Å}^{-1}$. Applying a tolerance of $\pm\ 0.05\,\text{Å}^{-1}$, the region of reciprocal space analyzed was set to $0.81\,\text{Å}^{-1} < q < 0.91\,\text{Å}^{-1}$ in order to isolate the signal associated with the (110) plane without including diffraction from other crystal planes. The diffraction intensity of (110) plane (centered at $q = 0.86\,\text{Å}^{-1}$) was plotted as a function of χ (the polar angle of the reciprocal space vector). Background signal was subtracted from the integrated intensity function prior to determining the degree of preferential orientation, defined in **Equation 1**:

$$Degree\ of\ Preferential\ Orientation = \frac{\int_{\chi=-54.8^\circ}^{\chi=-29.3^\circ} I_{110}(\chi)d\chi}{\int_{\chi=-90^\circ}^{\chi=0^\circ} I_{110}(\chi)d\chi} \qquad \textbf{(Equation 1)}$$

Where χ is the polar angle coordinate and I_{110} is the diffraction intensity associated with the (110) plane (see **SI Figure 7** for further discussion of variable definitions). In an oriented sample, the (110) peak center was determined to be at $\chi = -42.0°$. The full width at half max (FWHM) was found to be $12.8°$. Therefore, in the numerator, the limits of the integral to study orientation were established as the peak center ± FWHM ($-54.8° < \chi < -29.3°$). The full signal associated with the (110) plane ($-90° < \chi < 0°$) is expressed in the denominator. An example of this calculation is included in the supporting information.

RESULTS AND DISCUSSION

Solution shearing, a MGC technique, was used to create thin films of acetaminophen. Using an acetaminophen/water solution at a concentration of 10 mg mL^{-1}, we assessed crystal morphology in a parameter space consisting of coating speeds ranging from 0.03 - 3 mm s^{-1} and temperatures ranging from 70 - 120 °C. **Figure 1** shows the resultant processing diagram that presents regions where distinct morphologies of acetaminophen were isolated based on coating speed and temperature. We found three thin film morphologies, which are localized in discrete regions (annotated in **Figure 1**) on the processing diagram. In region 1, spherulitic crystals (**Figure 2a**) are obtained with fast coating speeds (0.3 mm s^{-1} and greater) across all temperatures. Spherulitic morphology was also obtained at a lower speed of 0.1 mm s^{-1} at a

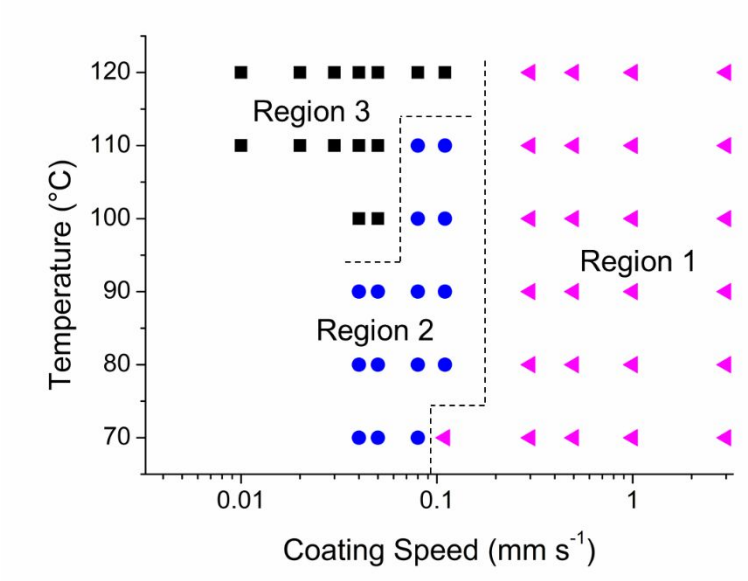

Figure 1: Processing diagram with coating conditions, created by varying coating speed and substrate temperature for a starting concentration of 10 mg mL^{-1}. Diagram with three regions of thin film morphology which are described as spherulitic crystals (region 1), non-uniform deposits (region 2) and microcrystals (region 3).

temperature of 70°. In this region, the crystallization process is decoupled from the film deposition process; the film that is originally deposited is amorphous, and transitions to a crystalline film over time when stored at room temperature. The transformation to a crystalline film occurred on a relatively short timescale (minutes) after film deposition.[27] Spherulitic morphology emerges from radial crystal growth from a central nucleation point. Therefore, there is no preferential direction to crystal growth imposed.

Figure 2b shows the representative image of films created in region 2, which was obtained by decreasing the coating speed (0.03 - 0.3 mm s^{-1}) and operating at temperatures below 100 °C. Thin flm morphology created with these conditions is variable (referred to as non-uniform deposits), and there are breaks in the thin film, resulting in incomplete coverage of the substrate. For these non-uniform films, crystalline acetaminophen is deposited on the substrate followed by a region without a significant amount of acetaminophen, which is attributed in part to stick-slip motion of the fluid meniscus.[39]

The SEM image of non-uniform deposits shows that the films are composed of thick, faceted crystals. A bulk deposit of material is followed by a region of thinner film, with smaller crystals and some needle-like extensions (SEM in **Figure 2b**). We hypothesize that after the larger faceted crystals are deposited, there is depletion of acetaminophen monomers in solution at the meniscus where film deposition occurs. This creates a diffusion limited condition in the thinner film regions. The crystals are also elongated, due to the concentration gradient that exists during thin film formation in this coating regime.[40] While a slower coating speed (region 2) facilitated the formation of the crystalline film without the formation of an amorphous film first (as in region 1), these conditions did not produce desirable film coverage or low aspect ratio crystals.

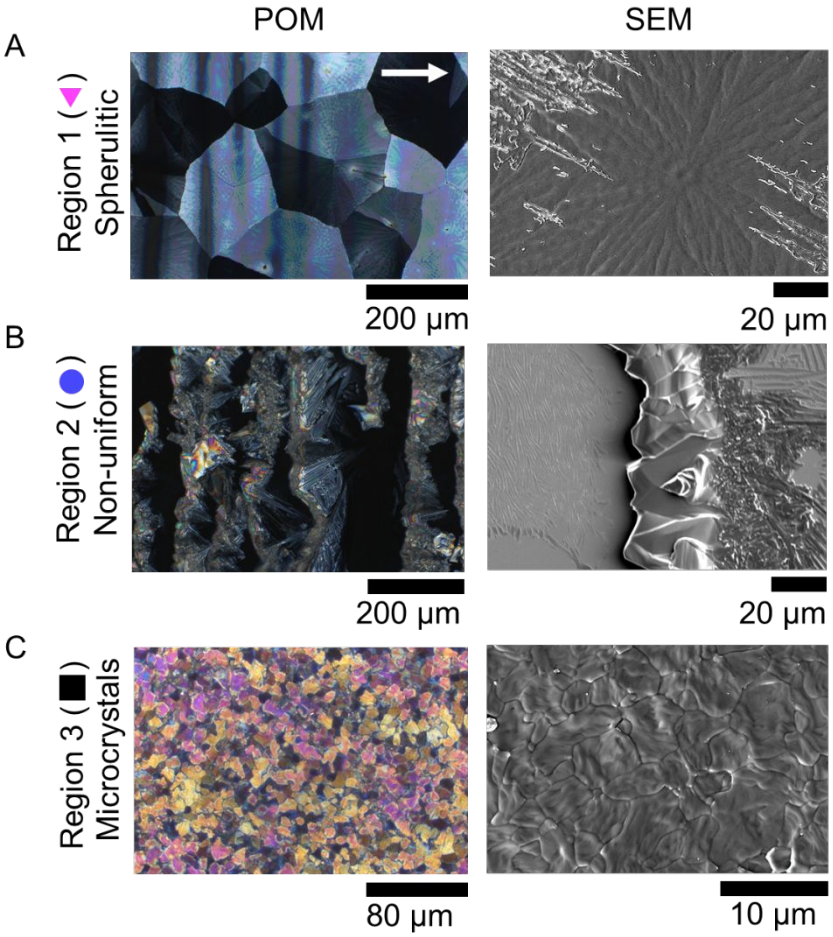

Figure 2: Polarized optical microscopy (POM) and scanning electron microscopy (SEM) of crystal morphologies, corresponding to three regions on processing diagram. a) Spherulitic films in region 1 b) non-uniform crystal films in region 2 and c) close packed microcrystal films in region 3.

In attempt to form a fully covered film, the substrate temperature was increased to 110 and 120 °C, which are above the boiling point of water, the working solvent. Accounting for a temperature drop from the heating source through the silicon substrate, we hypothesized that increasing the temperature (to 110 °C and 120 °C) would allow us to access evaporation at or above the solvent boiling point. Using this set of processing conditions produces the morphology, observed in region 3, where we isolated films comprised of microcrystals with highly uniform size and resulting in full film coverage (**Figure 2c**). SEM shows that the microcrystal films comprise close-packed crystallites with only slight thickness variation across the film and within individual crystallites. Each of these morphologies are distinct from the crystal morphology observed using dropcasting (**SI Figure 2**). Changing processing conditions during MGC allowed us to isolate unique three crystal morphologies. Most notably, it allowed us to discover a morphological regime for microcrystal production.

To the authors' knowledge, there is not another report of using coating temperatures that exceed the boiling point of the solvent to modulate particle morphology during film deposition. This microcrystal morphology (regime 3) is in contrast to aligned crystal morphology typically observed from solution shearing. MGC processes are predominantly utilized in the field of organic electronics and photovoltaics.[41] In these applications, the ideal crystal morphology is given by the coherence and alignment of a large crystalline domain; this crystal domain alignment facilitates charge transport in organic semiconductors.[42] Therefore, typical operational parameters for solution shearing are designed to achieve such characteristics.[43] However, when utilizing the technology for pharmaceutical crystallization, it is necessary to reassess ideal film morphology characteristics. As a result, sampling a new set of conditions (high temperature and slow coating speeds) allowed this work to identify a regime for microcrystal formation.

To explore the limitations of this technique for creating microcrystals, we extended the analysis to include higher (14 mg mL^{-1}) and lower (1 and 5 mg mL^{-1}) starting concentrations of acetaminophen; these concentrations are at and below the solubility limit of acetaminophen in

water at 23°C (**SI Figure 3**), respectively.[44] We found that microcrystals were isolated at 14, 10 and 5 mg mL^{-1} conditions, but reducing the concentration to 1 mg mL^{-1} produced films with larger crystallites (**Figure 3**). We hypothesize that below a critical concentration, the supersaturation required for the precipitation regime cannot be reached fast enough so more crystal growth occurs resulting in larger crystallites.

We hypothesized that the changes in crystal morphology are closely related to the coating regime and the associated relative timescales of evaporation and film deposition.[45] Therefore, it was of interest to characterize the coating regime and compare it to traditionally understood theory surrounding solution shearing. Solution shearing and other MGC techniques utilize fluid flow and surface tension to create a uniform film. The shape of the meniscus is significant in directing film assembly, and frequently, the coating regime is characterized through relating the change in film thickness with the coating speed.[23,46] Described extensively in literature, slow coating speeds are associated with an evaporative coating regime, where the coating speed is inversely proportional

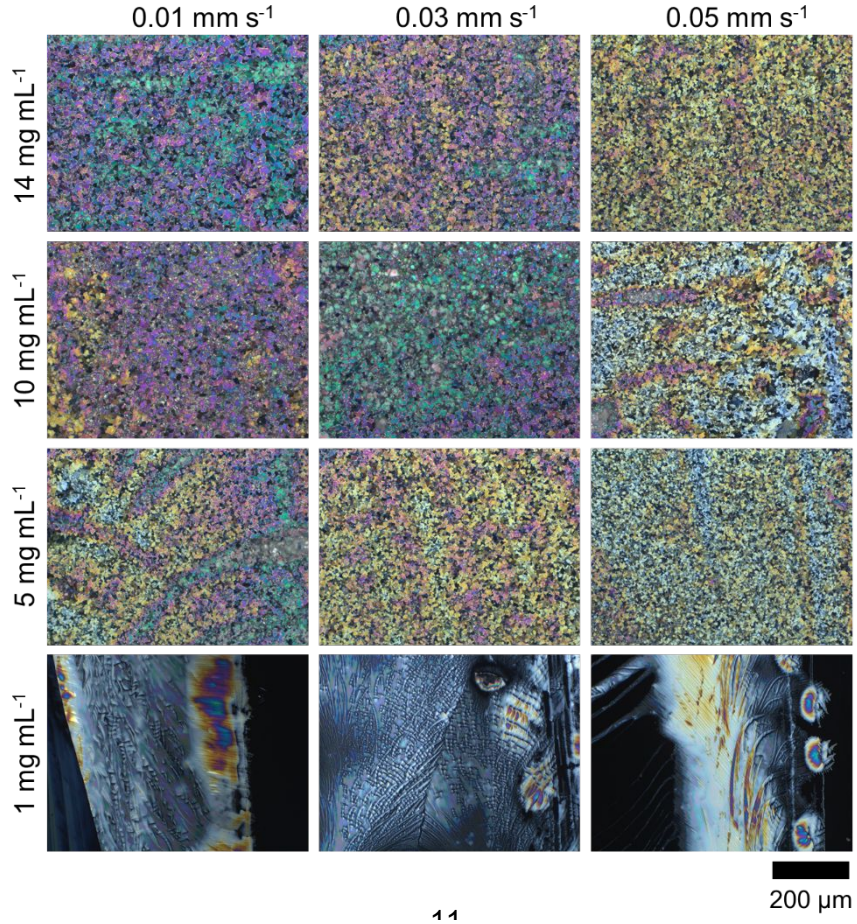

Figure 3: Microcrystals are isolated at 5, 10, 14 mg mL^{-1} starting solution concentrations but not at 1 mg mL^{-1}. Scale bar is 200 µm for all images.

to the film thickness (thickness $\propto$ speed^{-1}).[23] Faster coating speeds are associated with the Landau-Levich coating regime, where the film thickness and coating speed are positively correlated (thickness $\propto$ speed$^{2/3}$).[23]

The coating regime for microcrystal thin films (region 3, **Figure 1**) was characterized by determining the relationship between film thickness and coating speed. In **Figure 4a**, for all concentrations tested, the films are microns thick (2.99 ± 1.02 μm across all samples) and do not have a thickness dependence on either starting concentration or film coating speed. Creating a log-log plot of the thickness as a function of coating speed and performing a linear fit, there does not appear to be an inverse relationship between film thickness and coating speed, as would occur in the evaporative regime (**SI Figure 4**). For the initial concentrations of 5, 10, and 14 mg mL^{-1}, operating at slow coating speeds (0.01 - 0.05 mm s^{-1}) and elevated temperature (120 °C) produced films with thicknesses that do not follow the trends of the evaporative or Landau-Levich regimes. In fact, the coating speed does not appear to be a significant predictor of film thickness under these processing conditions. Due to the high temperatures, it is possible that a steady state meniscus is not achieved in this region due to the rapid evaporation.

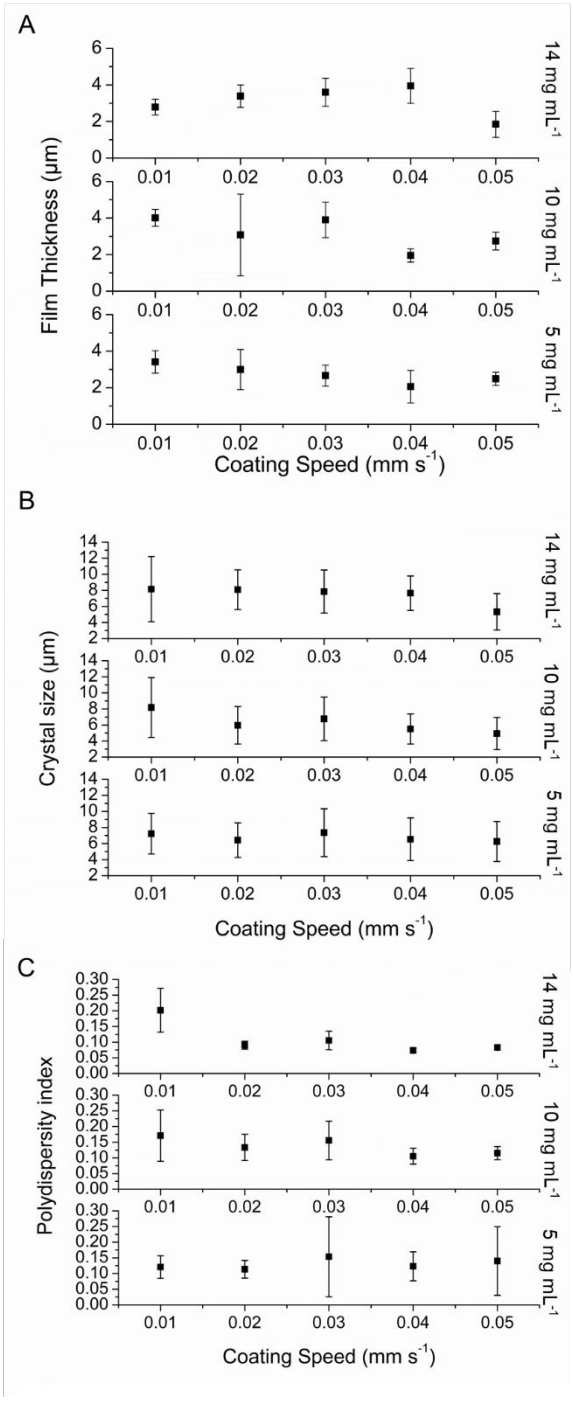

Figure 4: Film thickness (a), crystal sizes (b) and polydispersity (c) of samples fabricated at 5, 10, and 14 mg mL^{-1} concentrations, with coating speeds from 0.01 - 0.05 mm s^{-1}.

We hypothesize that the morphological results described here are a result of the fast evaporation relative to film deposition ($\tau_{\text{deposition}} > \tau_{\text{evaporation}}$). At temperatures above the boiling point of the solvent, the meniscus recedes and decouples the coating process such that the coating speed is not a significant parameter to control the film thickness. The fast evaporation rate causes rapid nucleation, which allows for the formation of small microcrystals. Therefore, we have identified a new application of the solution coating technique for the production of microcrystals, facilitated by the use of fast evaporation relative to the timescale of film deposition.

The change in microcrystal size was investigated as a function of coating speed and the initial solution concentration. The coating speed was varied from 0.01 - 0.05 mm s^{-1}, with concentrations of 5, 10 and 14 mg mL^{-1} since these conditions consistently produced the desired microcrystal film morphology. Crystal size distributions (CSDs) were plotted on histograms and the average crystal size was found for each population (**SI Figure 5**).

The microcrystals were analyzed to determine the average crystal size and the polydispersity, $PDI = \left(\frac{Standard\ Deviation}{Average}\right)^2$. We found that crystal sizes are not predictably different when changing processing conditions or the starting concentrations, and that most samples contained a similar distribution of crystal sizes, with the average size being 6.9 ± 2.4 μm across all samples (**Figure 4b, SI Table 1, SI Table 2, SI Table 3**). A polydispersity index of < 0.1 is an indication that the distribution of particles is monodisperse, i.e. most crystals are of the same size (**Figure 4c**).[33,47] We found that the PDI of microcrystal samples for a set of conditions can be less than 0.1, with the average PDI across all conditions being 0.13. This indicates that it is possible to obtain a monodisperse CSD, however there may be some variation from sample to sample.

Most applications of MGC in region 1 and 2 (which utilize moderate temperatures and faster coating speeds) achieve control over crystal alignment through controlling crystal growth after limited nucleation events.[29,42] In region 3 the microcrystals obtained appear to be formed through reaching a processing condition that favors nucleation over growth. Further, because we

do not observe significant change in microcrystal size across different processing conditions (speed, temperature and concentration), we hypothesize that the crystal growth must be limited, such that nucleation is the primary contributor to the final crystal size. This is similar to other methods of achieving precipitation, such as spray drying.[48] Reducing the starting concentration to 1 mg mL^{-1} prevents the system from reaching supersaturation fast enough to achieve high nucleation rates.

Finally, X-ray diffraction was used to understand the crystallization behavior, such as polymorphism and crystal texture in thin films, as well as to understand whether homogenous or heterogeneous nucleation occurs as a mechanism for crystallization in the different processing regimes from **Figure 1**. Polymorphism was determined by comparison of XRD patterns to

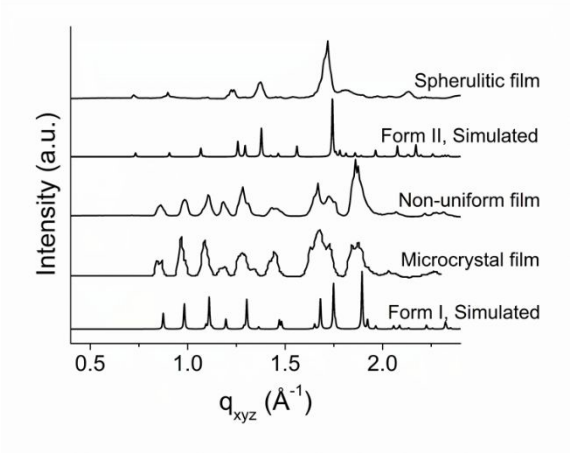

Figure 5: Representative XRD patterns of spherulitic, non-uniform and microcrystal crystal morphologies and simulated patterns for Form I and Form II of acetaminophen.

previously published data for Form I and Form II of acetaminophen.[36,37] From region 1, the spherulitic crystals were found to be Form II while the films from regions 2 and 3 were both composed of Form I (**Figure 5**).[27] We refrain from extensive analysis of the polymorphism in this study, as it was discussed in our previous work.[27]

The use of an area detector and a synchrotron X-ray source enabled us to observe the film texture associated with the different crystal morphologies. Interestingly, while processing regions 2 and 3 contained the same polymorph (form I), the film textures were distinct.

The diffraction from films in region 3 appears in localized regions consistent with preferential orientation of crystals on the substrate (**Figure 6a**).[49] Using peak indexing, we found that the (010) plane lies parallel to the substrate (**SI Figure 6**). However, the films from region 2 (non-uniform morphology) (**Figure 6b**) exhibit diffraction that is dispersed (i.e. without preferential orientation) along the annular rings of constant q, which is associated with randomly oriented crystals.

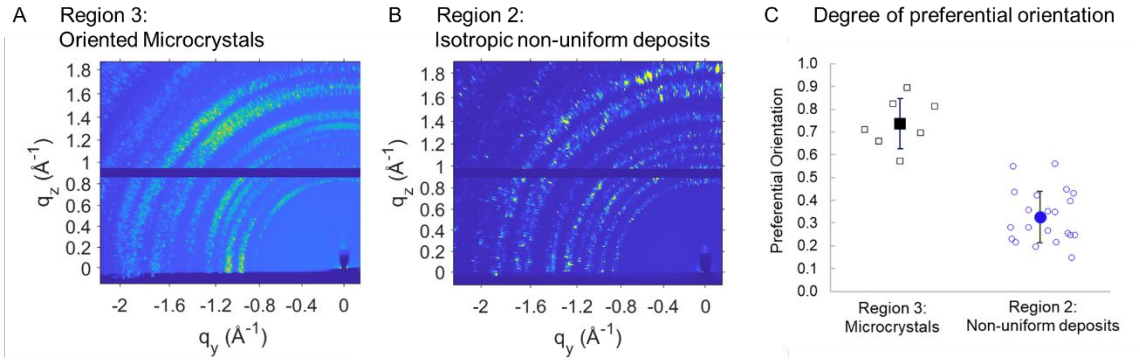

Figure 6: a) Microcrystal thin films exhibit preferential orientation. b) Films composed of non-uniform deposits are not oriented with respect to the substrate. c) Microcrystal films (n = 7, average = 0.74, stdev = 0.11) and non-uniform films (n = 22, average = 0.33, stdev = 0.11) show different degrees of preferential orientation, calculated using **Equation 1**. Groups are statistically different (p-value < 0.05). Sample processing conditions are in SI Table 4 and SI Table 5.

To more thoroughly quantify the difference in crystal texture, we used **equation 1** to measure the degree of preferential orientation of crystals with respect to the substrate (**SI Figure 7**). The samples created in regions 2 (non-uniform) and 3 (microcrystals) were divided into two populations according to the observed morphology: films composed of microcrystal morphology and films composed of the non-uniform deposits. Shown in **Figure 6c**, the average preferential orientation value for region 3 was 0.74 ± 0.11 (**SI Table 4**) while the samples from region 2 had lower preferential orientation with an average value of 0.33 ± 0.11 (**SI Table 5**). The populations were found to be significantly different (p-value < 0.05). The average of the non-uniform deposit samples is similar to the theoretical value associated with an isotropic sample, exhibiting no preferential orientation. This points towards heterogeneous nucleation as the prevalent

mechanism of crystallization to produce the close packed and oriented microcrystals in processing region 3.

Heterogeneous nucleation refers to nucleation that happens at an interface, as opposed to homogeneous nucleation that occurs in solution.[50,51] Previous work by Chen et al. has shown that heterogeneous nucleation can be responsible for directing crystal orientation in thin films.[38] The diffraction patterns in **Figure 6** can be described by heterogeneous nucleation for the case of preferentially oriented films from processing region 3 (**Figure 6a**). The presence of an interface acts to decrease the energetic barrier to nucleation, leading to nucleation on the interface, namely heterogeneous nucleation.[50] In processing region 3, we observed nucleation dominated crystallization, which is consistent with heterogeneous nucleation, where the reduced energetic barrier to nucleation could promote many nucleation events, leading to the formation of microcrystals.

CONCLUSION

This work demonstrates a novel utilization of solution shearing by using new crystallization conditions to create thin film microcrystals with low aspect ratios for acetaminophen from aqueous solutions. We identified a previously unobserved crystal morphology by accessing unique processing conditions, using slow coating speeds and high processing temperature (substrate temperature greater than the boiling point of the solvent).

We characterized the films comprised of microcrystals, including the polymorphic identity, the film thickness, crystal size distributions and polydispersity. Through this, we identify 1) a unique correlation of film thickness with coating speed and 2) the crystallization regime that is similar to precipitation, where nucleation is heavily favored over crystal growth. These observations lead us to conclude that a new crystallization regime during MGC was accessed, which we identify as a precipitation crystallization regime. The knowledge gained from these experiments could be scaled up to continuous and industrial scales in order to facilitate the production of crystals with controlled morphology and polymorphism.

Microcrystals are of particular interest in the pharmaceutical industry because the size and shape are amenable to fast dissolution, and the flowability of this shape is desirable compared to needles or plates.[13,15] Also of interest, but not explored in this work is the impact of the solvent choice and additives or impurities on film morphology; solvent polarity, pH, boiling point and evaporation rate can impact molecular assembly, leading to different supersaturation conditions during crystallization. Supersaturation is a critical factor that directs nucleation and growth, which in turn dictates polymorphism and crystal habit formation. Solvent selection is well studied in bulk crystallization of acetaminophen.[52–55] There also literature that explores the impact of solvent selection on organic semiconductor crystallization and polymer deposition during MGC.[41,43,56] Therefore, the importance of solvent selection should not be minimized or ignored in the context of pharmaceuticals during MGC and we invite other interested researchers to join in these investigations.

Future work will be directed towards understanding dissolution performance between different thin film morphologies, which requires more methodology and technological development and is thus outside of the scope of this work. Further, we aim to enable continuous crystallization by integration continuous solution feed with the MGC instrument, as this is a limiting factor in creating larger area films and scaling up production at the bench scale. The pharmaceutical industry is actively seeking tools to aid in the production of crystals with controllable size and shape. We posit that this processing method could be adopted and further explored for use in continuous crystallization processes. This novel regime of MGC may also be useful in other fields like organic semiconductors, perovskites, batteries, and even the food industry[38,57–59].

Acknowledgements

The Zygo NewView 7300 white light profilometer and FEI Quanta 650 scanning electron microscope utilized in this work are part of the University of Virginia Nanoscale Materials Characterization Facility.

This work is based upon research conducted at the Cornell High Energy Synchrotron Source (CHESS) at the D-1 Beamline. The work was supported by the National Science Foundation under award DMR-1332208.

S.G. and G.G. acknowledge financial support from the Thomas F. And Kate Miller Jeffress Memorial Trust, the University of Virginia School of Engineering and Applied Sciences and the Virginia Space Grant Consortium (NNX15A120H).

REFERENCES

(1) Mollan, M. J.; Lodaya, M. Continuous Processing in Pharmaceutical Manufacturing: Where We Have Been and Where We Are Going. *American Pharmaceutical Review*. 2004, pp 70–75.

(2) Mascia, S.; Heider, P. L.; Zhang, H.; Lakerveld, R.; Benyahia, B.; Barton, P. I.; Braatz, R. D.; Cooney, C. L.; Evans, J. M. B.; Jamison, T. F.; Jensen, K. F.; Myerson, A. S.; Trout, B. L. End-to-End Continuous Manufacturing of Pharmaceuticals: Integrated Synthesis, Purification, and Final Dosage Formation. *Angew. Chemie - Int. Ed.* **2013**, *52* (47), 12359–12363. https://doi.org/10.1002/anie.201305429.

(3) Yu, L. X.; Amidon, G.; Khan, M. A.; Hoag, S. W.; Polli, J.; Raju, G. K.; Woodcock, J. Understanding Pharmaceutical Quality by Design. *AAPS J.* **2014**, *16* (4), 771–783. https://doi.org/10.1208/s12248-014-9598-3.

(4) Brown, C. J.; Mcglone, T.; Yerdelen, S.; Srirambhatla, V.; Mabbott, F.; Gurung, R.; Briuglia, M. L.; Ahmed, B.; Polyzois, H.; Mcginty, J.; Perciballi, F.; Fysikopoulos, D.; Macfhionnghaile, P.; Siddique, H.; Raval, V.; Harrington, T. S.; Vassileiou, A. D.; Robertson, M.; Prasad, E.; Johnston, A.; Johnston, B.; Nordon, A.; Srai, J. S.; Halbert, G.; Ter Horst, J. H.; Price, C. J.; Rielly, C. D.; Sefcik, J.; Florence, A. J. Enabling Precision Manufacturing of Active Pharmaceutical Ingredients: Workflow for Seeded Cooling Continuous Crystallisations. *Mol. Syst. Des. Eng.* **2018**, *3* (3), 518–549.

https://doi.org/10.1039/c7me00096k.

(5) Wang, T.; Lu, H.; Wang, J.; Xiao, Y.; Zhou, Y.; Bao, Y.; Hao, H. Recent Progress of Continuous Crystallization. *J. Ind. Eng. Chem.* **2017**, *54*, 14–29. https://doi.org/10.1016/j.jiec.2017.06.009.

(6) Su, Q.; Nagy, Z. K.; Rielly, C. D. Pharmaceutical Crystallisation Processes from Batch to Continuous Operation Using MSMPR Stages: Modelling, Design, and Control. *Chem. Eng. Process. Process Intensif.* **2015**, *83*, 41–53. https://doi.org/10.1016/j.cep.2015.01.001.

(7) Poechlauer, P.; Manley, J.; Broxterman, R.; Gregertsen, B.; Ridemark, M. Continuous Processing in the Manufacture of Active Pharmaceutical Ingredients and Finished Dosage Forms: An Industry Perspective. *Org. Process Res. Dev.* **2012**, *16* (10), 1586–1590. https://doi.org/10.1021/op300159y.

(8) Acevedo, D.; Yang, Y.; Warnke, D. J.; Nagy, Z. K. Model-Based Evaluation of Direct Nucleation Control Approaches for the Continuous Cooling Crystallization of Paracetamol in a Mixed Suspension Mixed Product Removal System. *Cryst. Growth Des.* **2017**, *17* (10), 5377–5383. https://doi.org/10.1021/acs.cgd.7b00860.

(9) Jiang, M.; Wong, M. H.; Zhu, Z.; Zhang, J.; Zhou, L.; Wang, K.; Ford Versypt, A. N.; Si, T.; Hasenberg, L. M.; Li, Y. E.; Braatz, R. D. Towards Achieving a Flattop Crystal Size Distribution by Continuous Seeding and Controlled Growth. *Chem. Eng. Sci.* **2012**, *77*, 2–9. https://doi.org/10.1016/j.ces.2011.12.033.

(10) Orehek, J.; Teslić, D.; Likozar, B. Continuous Crystallization Processes in Pharmaceutical Manufacturing: A Review. *Org. Process Res. Dev.* **2021**, *25* (1), 16–42. https://doi.org/10.1021/acs.oprd.0c00398.

(11) Taipale-Kovalainen, K.; Ketolainen, J.; Korhonen, O.; Ervasti, T. Converting a Batch Based High-Shear Granulation Process to a Continuous Dry Granulation Process; a Demonstration with Ketoprofen Tablets. *Eur. J. Pharm. Sci.* **2020**, *151* (105381). https://doi.org/10.1016/j.ejps.2020.105381.

(12) Rimez, B.; Debuysschère, R.; Conté, J.; Lecomte-Norrant, E.; Gourdon, C.; Cognet, P.; Scheid, B. Continuous-Flow Tubular Crystallization to Discriminate between Two Competing Crystal Polymorphs. 1. Cooling Crystallization. *Cryst. Growth Des.* **2018**, *18* (11), 6431–6439. https://doi.org/10.1021/acs.cgd.8b00928.

(13) Dizaj, S. M.; Vazifehasl, Z.; Salatin, S.; Adibkia, K.; Javadzadeh, Y. Nanosizing of Drugs: Effect on Dissolution Rate. *Res. Pharm. Sci.* **2015**, *10* (2), 95–108.

(14) Sigfridsson, K.; Lundqvist, A. J.; Strimfors, M. Particle Size Reduction and Pharmacokinetic Evaluation of a Poorly Soluble Acid and a Poorly Soluble Base during Early Development. *Drug Dev. Ind. Pharm.* **2011**, *37* (3), 243–251. https://doi.org/10.3109/03639045.2010.505927.

(15) Chatterjee, A.; Gupta, M.; Srivastava, B. Spherical Crystallization: A Technique Use to Reform Solubility and Flow Property of Active Pharmaceutical Ingredients. *Int. J. Pharm. Investig.* **2017**, *7* (1), 4–9. https://doi.org/10.4103/jphi.jphi_36_16.

(16) Moura, C.; Casimiro, T.; Costa, E.; Aguiar-Ricardo, A. Optimization of Supercritical CO2-Assisted Spray Drying Technology for the Production of Inhalable Composite Particles Using Quality-by-Design Principles. *Powder Technol.* **2019**, *357*, 387–397. https://doi.org/10.1016/j.powtec.2019.08.090.

(17) Kumar, S.; Shen, J.; Zolnik, B.; Sadrieh, N.; Burgess, D. J. Optimization and Dissolution Performance of Spray-Dried Naproxen Nano-Crystals. *Int. J. Pharm.* **2015**, *486* (1–2), 159–166. https://doi.org/10.1016/j.ijpharm.2015.03.047.

(18) Long, B.; Ryan, K. M.; Padrela, L. Investigating Process Variables and Additive Selection to Optimize Polymorphic Control of Carbamazepine in a CO2Antisolvent Crystallization Process. *Org. Process Res. Dev.* **2020**, *24* (6), 1006–1017. https://doi.org/10.1021/acs.oprd.9b00545.

(19) Werzer, O.; Baumgartner, R.; Zawodzki, M.; Roblegg, E. Particular Film Formation of Phenytoin at Silica Surfaces. *Mol. Pharm.* **2014**, *11* (2), 610–616. https://doi.org/10.1021/mp4006479.

(20) Ehmann, H. M. A.; Werzer, O. Surface Mediated Structures: Stabilization of Metastable Polymorphs on the Example of Paracetamol. *Cryst. Growth Des.* **2014**, *14* (8), 3680–3694. https://doi.org/10.1021/cg500573e.

(21) Werzer, O.; Tumphart, S.; Keimel, R.; Christian, P.; Coclite, A. M. Drug Release from Thin Films Encapsulated by a Temperature-Responsive Hydrogel. *Soft Matter* **2019**, *15* (8), 1853–1859. https://doi.org/10.1039/C8SM02529K.

(22) Lu, Z.; Wang, C.; Deng, W.; Achille, M. T.; Jie, J.; Zhang, X. Meniscus-Guided Coating of Organic Crystalline Thin Films for High-Performance Organic Field-Effect Transistors. *J. Mater. Chem. C* **2020**, *8* (27), 9133–9146. https://doi.org/10.1039/D0TC01887B.

(23) Le Berre, M.; Chen, Y.; Baigl, D. From Convective Assembly to Landau - Levich Deposition of Multilayered Phospholipid Films of Controlled Thickness. *Langmuir* **2009**, *25* (5), 2554–2557. https://doi.org/10.1021/la803646e.

(24) Giri, G.; Verploegen, E.; Mannsfeld, S. C.; Atahan-Evrenk, S.; Kim do, H.; Lee, S. Y.; Becerril, H. A.; Aspuru-Guzik, A.; Toney, M. F.; Bao, Z. Tuning Charge Transport in Solution-Sheared Organic Semiconductors Using Lattice Strain. *Nature* **2011**, *480* (7378), 504. https://doi.org/10.1038/nature10683.

(25) Giri, G.; Delongchamp, D. M.; Reinspach, J.; Fischer, D. A.; Richter, L. J.; Xu, J.; Benight, S.; Ayzner, A.; He, M.; Fang, L.; Xue, G.; Toney, M. F.; Bao, Z. Effect of Solution Shearing Method on Packing and Disorder of Organic Semiconductor Polymers. *Chem. Mater.* **2015**, *27* (7), 2350–2359. https://doi.org/10.1021/cm503780u.

(26) Pascoe, A. R.; Gu, Q.; Rothmann, M. U.; Li, W.; Zhang, Y.; Scully, A. D.; Lin, X.; Spiccia, L.; Bach, U.; Cheng, Y. B. Directing Nucleation and Growth Kinetics in Solution-Processed Hybrid Perovskite Thin-Films. *Sci. China Mater.* **2017**, No. 60, 617–628. https://doi.org/10.1007/s40843-017-9043-y.

(27) Guthrie, S. M.; Smilgies, D. M.; Giri, G. Controlling Polymorphism in Pharmaceutical Compounds Using Solution Shearing. *Cryst. Growth Des.* **2018**, *18* (2), 602–606. https://doi.org/10.1021/acs.cgd.7b01686.

(28) Horstman, E. M.; Kafle, P.; Zhang, F.; Zhang, Y.; Kenis, P. J. A. A.; Diao, Y. Solution Coating of Pharmaceutical Nanothin Films and Multilayer Nanocomposites with Controlled Morphology and Polymorphism. *ACS Appl. Mater. Interfaces* **2018**, *10* (12), 10480–10489. https://doi.org/10.1021/acsami.8b01074.

(29) Diao, Y.; Shaw, L.; Bao, Z.; Mannsfeld, S. C. B. Morphology Control Strategies for Solution-Processed Organic Semiconductor Thin Films. *Energy Environ. Sci.* **2014**, *7*, 2145–2159. https://doi.org/10.1039/c4ee00688g.

(30) Karki, S.; Kim, H.; Na, S. J.; Shin, D.; Jo, K.; Lee, J. Thin Films as an Emerging Platform for Drug Delivery. *Asian J. Pharm. Sci.* **2016**, *11* (5), 559–574. https://doi.org/10.1016/j.ajps.2016.05.004.

(31) Khadra, I.; Obeid, M. A.; Dunn, C.; Watts, S.; Halbert, G.; Ford, S.; Mullen, A. Characterisation and Optimisation of Diclofenac Sodium Orodispersible Thin Film Formulation. *Int. J. Pharm.* **2019**, *561*, 43–46.

https://doi.org/10.1016/j.ijpharm.2019.01.064.

(32) Schlesinger, E.; Ciaccio, N.; Desai, T. A. Polycaprolactone Thin-Film Drug Delivery Systems: Empirical and Predictive Models for Device Design. *Mater. Sci. Eng. C* **2015**, *57*, 232–239. https://doi.org/10.1016/j.msec.2015.07.027.

(33) Clayton, K. N.; Salameh, J. W.; Wereley, S. T.; Kinzer-Ursem, T. L. Physical Characterization of Nanoparticle Size and Surface Modification Using Particle Scattering Diffusometry. *Biomicrofluidics* **2016**, *10* (5), 054107. https://doi.org/10.1063/1.4962992.

(34) Danaei, M.; Dehghankhold, M.; Ataei, S.; Hasanzadeh Davarani, F.; Javanmard, R.; Dokhani, A.; Khorasani, S.; Mozafari, M. R. Impact of Particle Size and Polydispersity Index on the Clinical Applications of Lipidic Nanocarrier Systems. *Pharmaceutics* **2018**, *10* (2), 57. https://doi.org/10.3390/pharmaceutics10020057.

(35) Smilgies, D. M.; Blasini, D. R. Indexation Scheme for Oriented Molecular Thin Films Studied with Grazing-Incidence Reciprocal-Space Mapping. *J. Appl. Crystallogr.* **2007**, *40* (4), 716–718. https://doi.org/10.1107/S0021889807023382.

(36) Nelyubina, Y. V.; Glukhov, I. V.; Antipin, M. Y.; Lyssenko, K. A. “higher Density Does Not Mean Higher Stability” Mystery of Paracetamol Finally Unraveled. *Chem. Commun.* **2010**, *46* (20), 3469–3471. https://doi.org/10.1039/b927429d.

(37) Nichols, G.; Frampton, C. S. Physicochemical Characterization of the Orthorhombic Polymorph of Paracetamol Crystallized from Solution. *J. Pharm. Sci.* **1998**, *87* (6), 684–693. https://doi.org/10.1021/js970483d.

(38) Chen, A. Z.; Shiu, M.; Ma, J. H.; Alpert, M. R.; Zhang, D.; Foley, B. J.; Smilgies, D. M.; Lee, S. H.; Choi, J. J. Origin of Vertical Orientation in Two-Dimensional Metal Halide Perovskites and Its Effect on Photovoltaic Performance. *Nat. Commun.* **2018**, *9* (1), 1–7.

https://doi.org/10.1038/s41467-018-03757-0.

(39) Abo Jabal, M.; Egbaria, A.; Zigelman, A.; Thiele, U.; Manor, O. Connecting Monotonic and Oscillatory Motions of the Meniscus of a Volatile Polymer Solution to the Transport of Polymer Coils and Deposit Morphology. *Langmuir* **2018**, *34* (39), 11784–11794. https://doi.org/10.1021/acs.langmuir.8b02268.

(40) Zhang, Z.; Peng, B.; Ji, X.; Pei, K.; Chan, P. K. L. Marangoni-Effect-Assisted Bar-Coating Method for High-Quality Organic Crystals with Compressive and Tensile Strains. *Adv. Funct. Mater.* **2017**, *27* (37), 1703443. https://doi.org/10.1002/adfm.201703443.

(41) Gu, X.; Shaw, L.; Gu, K.; Toney, M. F.; Bao, Z. The Meniscus-Guided Deposition of Semiconducting Polymers. *Nat. Commun.* **2018**, *9*, 534. https://doi.org/10.1038/s41467-018-02833-9.

(42) Park, S.; Giri, G.; Shaw, L.; Pitner, G.; Ha, J.; Koo, J. H.; Gu, X.; Park, J.; Lee, T. H.; Nam, J. H.; Hong, Y.; Bao, Z. Large-Area Formation of Self-Aligned Crystalline Domains of Organic Semiconductors on Transistor Channels Using CONNECT. *Proc. Natl. Acad. Sci. U. S. A.* **2015**, *112* (18), 2–7. https://doi.org/10.1073/pnas.1419771112.

(43) Janneck, R.; Vercesi, F.; Heremans, P.; Genoe, J.; Rolin, C. Predictive Model for the Meniscus-Guided Coating of High-Quality Organic Single-Crystalline Thin Films. *Adv. Mater.* **2016**, *28* (36), 8007–8013. https://doi.org/10.1002/adma.201602377.

(44) Granberg, R. A.; Rasmuson, Å. C. Solubility of Paracetamol in Pure Solvents. *J. Chem. Eng. Data* **1999**, *46* (6), 1391–1395. https://doi.org/10.1021/je990124v.

(45) Michels, J. J.; Zhang, K.; Wucher, P.; Beaujuge, P. M.; Pisula, W.; Marszalek, T. Predictive Modelling of Structure Formation in Semiconductor Films Produced by Meniscus-Guided Coating. *Nat. Mater.* **2020**, 1–8. https://doi.org/10.1038/s41563-020-

0760-2.

(46) Zhang, K.; Wang, Z.; Marszalek, T.; Borkowski, M.; Fytas, G.; Blom, P. W. M.; Pisula, W. Key Role of the Meniscus Shape in Crystallization of Organic Semiconductors during Meniscus-Guided Coating. *Mater. Horizons* **2020**, *7*, 1631–1640. https://doi.org/10.1039/d0mh00141d.

(47) Hughes, J. M.; Budd, P. M.; Grieve, A.; Dutta, P.; Tiede, K.; Lewis, J. Highly Monodisperse, Lanthanide-Containing Polystyrene Nanoparticles as Potential Standard Reference Materials for Environmental “Nano” Fate Analysis. *J. Appl. Polym. Sci.* **2015**, *132* (24), 42061. https://doi.org/10.1002/app.42061.

(48) Yıldız, Ö. Combined Precipitation and Spray Drying for the Synthesis of Hydroxyapatite Nanopowders as Soft Spherical Granules. *Ceram. Int.* **2018**, *44* (16), 19809–19817. https://doi.org/10.1016/j.ceramint.2018.07.238.

(49) Widjonarko, N. Introduction to Advanced X-Ray Diffraction Techniques for Polymeric Thin Films. *Coatings* **2016**, *6* (4), 54. https://doi.org/10.3390/coatings6040054.

(50) Khaleghi, A.; Sadrameli, S. M.; Manteghian, M. Thermodynamic and Kinetics Investigation of Homogeneous and Heterogeneous Nucleation. *Rev. Inorg. Chem.* **2020**, *40* (4). https://doi.org/10.1515/revic-2020-0004.

(51) Markov, I. V. Chapter 2: Nucleation. In *Crystal Growth For Beginners: Fundamentals Of Nucleation, Crystal Growth And Epitaxy*; World Scientific, 2016.

(52) Li, J.; Doherty, M. F. Steady State Morphologies of Paracetamol Crystal from Different Solvents. *Cryst. Growth Des.* **2017**, *17* (2), 659–670. https://doi.org/10.1021/acs.cgd.6b01510.

(53) Kaialy, W.; Larhrib, H.; Chikwanha, B.; Shojaee, S.; Nokhodchi, A. An Approach to

Engineer Paracetamol Crystals by Antisolvent Crystallization Technique in Presence of Various Additives for Direct Compression. *Int. J. Pharm.* **2014**, *464* (1–2), 53–64. https://doi.org/10.1016/j.ijpharm.2014.01.026.

(54) Urwin, S. J.; Yerdelen, S.; Houson, I.; ter Horst, J. H. Impact of Impurities on Crystallization and Product Quality: A Case Study with Paracetamol. *Crystals*. 2021, p 1244. https://doi.org/10.3390/cryst11111344.

(55) Omar, W.; Al-Sayed, S.; Sultan, A.; Ulrich, J. Growth Rate of Single Acetaminophen Crystals in Supersaturated Aqueous Solution under Different Operating Conditions. *Cryst. Res. Technol.* **2008**, *43* (1), 22–27. https://doi.org/10.1002/crat.200710995.

(56) Giri, G.; Li, R.; Smilgies, D. M.; Li, E. Q.; Diao, Y.; Lenn, K. M.; Chiu, M.; Lin, D. W.; Allen, R.; Reinspach, J.; Mannsfeld, S. C. B.; Thoroddsen, S. T.; Clancy, P.; Bao, Z.; Amassian, A. One-Dimensional Self-Confinement Promotes Polymorph Selection in Large-Area Organic Semiconductor Thin Films. *Nat. Commun.* **2014**, *5*, 3573. https://doi.org/10.1038/ncomms4573.

(57) Foley, B. J.; Cuthriell, S.; Yazdi, S.; Chen, A. Z.; Guthrie, S. M.; Deng, X.; Giri, G.; Lee, S.-H.; Xiao, K.; Doughty, B.; Ma, Y.-Z.; Choi, J. J. Impact of Crystallographic Orientation Disorders on Electronic Heterogeneities in Metal Halide Perovskite Thin Films. *Nano Lett.* **2018**, *18* (10), 6271–6278. https://doi.org/10.1021/acs.nanolett.8b02417.

(58) Zhang, L.; Chen, L.; Zhou, X.; Liu, Z. Morphology-Dependent Electrochemical Performance of Zinc Hexacyanoferrate Cathode for Zinc-Ion Battery. *Sci. Rep.* **2015**, *5* (18263). https://doi.org/10.1038/srep18263.

(59) Quilaqueo, M.; Duizer, L.; Aguilera, J. M. The Morphology of Salt Crystals Affects the Perception of Saltiness. *Food Res. Int.* **2015**, *76* (3), 675–681. https://doi.org/10.1016/j.foodres.2015.07.004.